

Identifying trivial and Majorana zero-energy modes using the Majorana polarization

Oladunjoye A. Awoga^{1,*} and Jorge Cayao^{2,†}

¹*Division of Solid State Physics and NanoLund, Lund University, Box 118, 22100 Lund, Sweden*

²*Department of Physics and Astronomy, Uppsala University, Box 516, S-751 20 Uppsala, Sweden*

(Dated: October 4, 2024)

In this work we consider superconductor-semiconductor hybrids containing both trivial and Majorana zero modes and explore their signatures in the Majorana polarization. In particular, we consider trivial zero energy states due to confinement and disorder, which seem to be very likely experimental scenarios. We show that the Majorana polarization is able to characterize the topological phase transition as well as the emergence of Majorana zero modes even when trivial zero-energy states proliferate. Notably, the Majorana polarization inherits direct information about spatial correlations which are then the key for distinguishing Majorana and trivial zero-modes. We demonstrate the utility of the Majorana polarization in normal-superconductor junctions and superconductor-normal-superconductor Josephson junctions. Our results support the interpretation of the Majorana polarization as a real space topological indicator.

I. INTRODUCTION

Majorana zero modes (MZMs) emerge as zero-energy edge states in topological superconductors, a topological phase that has been predicted to occur in superconductor-semiconductor systems at strong Zeeman fields [1–4]. Since its conception, this idea has motivated an impressive amount of theoretical and experimental works searching for Majorana signatures [5–10] but it is still unclear whether MZMs have been observed or not [11]. The main issue was shown to be the proliferation of trivial zero-energy states (TZESs) well below the expected topological phase transition [12–24], with signatures similar to those due to MZMs [25–30]. This in turn has motivated intense efforts aiming at distinguishing between MZMs and TZESs [22, 31–35] but the problem is far from being settled [11].

In this work we show that the Majorana polarization, which characterizes the expectation value of the particle-hole operator, can be used as a real space topological indicator that distinguishes between MZMs and TZESs in superconducting systems [Fig. 1]. The Majorana polarization was used before to characterize MZMs but in the absence of TZESs [36–40]. The Majorana polarization was initially defined as an absolute value function and involved only over one half of the system. As such, this initial definition of the Majorana polarization is unable to distinguish between MZMs and TZESs and cannot capture the nonlocal correlations between MZMs (Majorana nonlocality) which involves having both ends of the system. We extend the previous definition and introduce the Majorana polarization as a quantity that captures the correlation between MZMs emerging at the edges, and eliminate the use of absolute value. To show the usefulness of the Majorana polarization, we first consider a finite superconductor with spin-orbit coupling under the

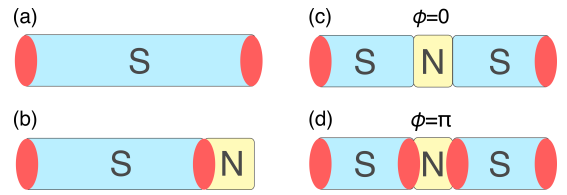


Figure 1. Sketch of the three superconducting systems with SOC and Zeeman field considered in this work. Panel (a) shows a superconductor S, while (b) a SN junction, in both cases with MZMs at the edges of S. Panels (c,d) depict a short SNS junction with two MZMs at $\phi = 0$ and four MZMs at $\phi = \pi$. The superconducting region (S) is indicated by cyan color, while the normal region (N) by yellow color.

presence of a Zeeman field and demonstrate that it detects the topological phase transition and the emergence of MZMs. In this case, we find that the Majorana polarization exactly captures the behavior of the Pfaffian, which then enables us to interpret the Majorana polarization as a real space topological indicator. Notably, we discover that the Majorana polarization remains a good topological invariant even under strong scalar disorder, where the visibility of the gap closing is degraded and an avalanche of disorder-induced TZESs emerge.

We then confirm the utility of the Majorana polarization to distinguish between MZMs and TZESs induced by confinement in normal-superconductor (NS) junctions and superconductor-normal-superconductor (SNS) Josephson junctions. In the SNS junction we also find that the Majorana polarization reveals the emergence of the two MZMs at $\phi = 0$ and four MZMs at $\phi = \pi$, which further support the interpretation of the Majorana polarization as a real space topological invariant. Since disorder and confinement effects represent two mechanisms that induce TZESs, and very likely present under realistic conditions, our results can be helpful for predicting the topological superconducting phase and MZMs in superconductor-semiconductor hybrid systems.

The remainder of this work is organized as follows. In

* oladunjoye.awoga@ftf.lth.se

† jorge.cayao@physics.uu.se

Section II we discuss the model and method, while in Section III we obtain the Majorana polarization in a finite nanowire without and with disorder. In Sections IV and V we show how the Majorana polarization distinguishes between TZESs and MZMs in NS and SNS junctions, respectively. Finally in Section VI, we present our conclusions. For completeness, in Appendix A we address the Majorana polarization in a minimal Kitaev chain, while in Appendix B we compare the Pfaffian and Majorana polarization in a disordered system.

II. MODELS AND METHOD

We consider three one-dimensional (1D) superconducting systems, including a finite superconductor, a NS junction, and a short SNS Josephson junction, as schematically shown in Fig. 1. We model these system by the following tight-binding Hamiltonian

$$\begin{aligned} \mathcal{H} = & \sum_{j=1, \sigma\sigma'}^M d_{j\sigma}^\dagger [\varepsilon(j)\delta_{\sigma\sigma'} + B\sigma_{\sigma\sigma'}^x + i\Delta(j)\sigma_{\sigma\sigma'}^y] d_{j\sigma'} \\ & + \sum_{j=1, \sigma\sigma'}^{M-1} d_{j\sigma}^\dagger [-t\delta_{\sigma\sigma'} + \alpha\sigma_{\sigma\sigma'}^y] d_{j+1, \sigma'} + \text{H.c.}, \end{aligned} \quad (1)$$

where $\varepsilon(j) = 2t - \mu(j) + V(j)$ is the site-dependent onsite energy with t being the nearest neighbor hopping amplitude, while $\mu(j)$ is the spatial dependent chemical potential and $V(j)$ a spatial dependent potential characterizing scalar disorder, which will be specified later. Here $d_{j\sigma}$ and $d_{j\sigma}^\dagger$, respectively, destroy and create a fermionic state with spin σ at site j in the superconducting system and runs over the entire system of length $L = Ma$, being M the total number of sites and a the lattice spacing. Moreover, in Eq. (1) α is the SOC strength, B the Zeeman field along x , and $\Delta(j)$ the space dependent superconducting pair potential. Thus, the finite superconductor in Fig. 1(a) of length L is described by an homogeneous pair potential $\Delta(j) = \Delta$ and finite chemical potential $\mu(j) = \mu$; the potential $V(j)$, however, still depends on space, see below. In this single superconducting nanowire, a topological phase transition occurs at $B = B_c$ where $B_c = \sqrt{\Delta^2 + \mu^2}$. Then, MZMs emerge when $B > B_c$, where the system becomes a p -wave superconductor and effectively describes the physics of the Kitaev chain [41].

To model the NS and SNS junctions in Fig. 1(b,c), the N region is considered to have $\Delta = 0$ and μ_N , while the S region $\Delta \neq 0$ and μ_S . We note that in the case of the SNS Josephson junction, we also consider a finite phase difference between the pair potentials of the S regions, such that we can explore the Josephson effect. The lengths of N (S) for these junctions are denoted as $L_{N(S)} = M_{N(S)}a$, where $M_{N(S)}$ correspond to the number of sites in the N(S) regions. Then, the S regions can become topological with MZMs at their ends for $B > B_c$.

We are interested in exploring the Majorana polarization to distinguish between MZMs and TZESs. Before discussing how to obtain the Majorana polarization, we point out that to characterize the topological phase of the Rashba model given by Eq. (1), it is common to use the Pfaffian topological invariant given by [42, 43]

$$\mathcal{M} = \text{sgn}[\text{Pf}[\tilde{\mathcal{H}}]] \quad (2)$$

where sgn represents the sign operation, Pf denotes the Pfaffian, and $\tilde{\mathcal{H}}$ is a skew-symmetric matrix obtained by writing the Hamiltonian in Eq. (1) in the Majorana basis, [41, 42, 44, 45]. We note that \mathcal{M} is sometimes referred to as Majorana number. To set a starting point in this work, we will use the Pfaffian to characterize the topological phase of the superconductor with homogeneous pair potential and modeled by Eq. (1). For this purpose, \mathcal{M} will be obtained in real space by taking periodic boundary conditions (closed system) such that the nanowire becomes a ring [45]. Thus, when MZMs emerge at the edges, under periodic boundary conditions, they hybridize and acquire finite energy. Furthermore, it is worth noting, however, the Pfaffian captures the fermion parity of the ground state. Thus, every time an energy level crosses zero, the parity of the system changes and therefore the Pfaffian changes sign, which is expected irrespective of either the trivial or topological nature of the system. Thus, in spite of the benefits of the Pfaffian as a bulk topological invariant, there is a need for an alternative metric to characterize the topological properties in real space, specially when the system is inhomogeneous and TZESs are present.

We argue that the issue with the Pfaffian in inhomogeneous systems can be resolved by using the Majorana polarization, which, as we show in this work, turns out to be a more powerful topological indicator because it allows to distinguish between MZMs and TZESs. For this reason, we start by defining the Majorana polarization at each site j as [37]

$$P_j \equiv \frac{\langle \Psi_j | \mathcal{C} | \Psi_j \rangle}{\langle \Psi_j | \Psi_j \rangle} = \frac{\sum_{\sigma=\uparrow, \downarrow} 2u_{j\sigma}^{(0)} [v_{j\sigma}^{(0)}]}{\sum_{\sigma=\uparrow, \downarrow} |u_{j\sigma}^{(0)}|^2 + |v_{j\sigma}^{(0)}|^2}, \quad (3)$$

where $\mathcal{C} = \tau^x \otimes \sigma^0 \mathcal{K}$ is the particle-hole operator, with \mathcal{K} the conjugation operator, τ^i and σ^i the i -th Pauli matrix in Nambu and spin spaces, respectively, while $u_{j\sigma}^{(0)}$ and $v_{j\sigma}^{(0)}$ represent the electron and hole components with spin σ of the wavefunction Ψ_j at site j of the lowest energy state. At this point, we anticipate that in a finite topological superconductor, the Majorana polarization P_j of the left and right halves of the system develop opposite signs. We show this effect by taking a two-site Kitaev chain at the sweet spot where MZMs appear, see Appendix A. Motivated by this fact, we take Eq. (3) and define the Majorana polarizations associated to the left and right half of the system, which we refer to as left (L) and right (R) Majorana polarizations and obtain them

as,

$$\begin{aligned}
 P_L &= \sum_{j=1}^{j=M/2} P_j, \\
 P_R &= \sum_{j=M/2+1}^{j=M} P_j.
 \end{aligned}
 \tag{4}$$

Then, given that P_L and P_R develop opposite signs in the presence of MZMs as anticipated above, we define a new quantity involving their multiplication as

$$\mathcal{P} = P_L^* \cdot P_R = P_L \cdot P_R^*,
 \tag{5}$$

which we refer to as *nonlocal* Majorana polarization because it simultaneously takes into account the behaviour of $P_{L/R}$. Note that, while $P_{L/R}$ is in general complex, \mathcal{P} is real. Since $P_{L/R}$ are normalized, the maximum absolute value they can take is unity, thus placing the nonlocal Majorana polarization within the range $\mathcal{P} \in [-1, 1]$: A value of $\mathcal{P} = -1$ implies that the MZMs are true zero-modes and do not overlap, whereas a slight deviation from $\mathcal{P} = -1$ corresponds that there is cross-talk between the MZMs or that there is a finite energy splitting of the MZMs energy. Any other value of \mathcal{P} signals a non Majorana state, namely, a topologically trivial state. With all these characteristics, it is expected that \mathcal{P} not only senses the topological transition but also measures the correlation between MZMs emerging at the edges of the system and, therefore, able to detect the Majorana spatial nonlocality. Following a similar spirit, the nonlocal Majorana polarization given by Eq. (5) can be easily generalized to higher dimensions, in the same way as the local Majorana polarization [37, 38]. Before going further, it is worth noting that, while the local Majorana polarization (3) is similar to the definition adopted in Refs. [37, 38], the nonlocal polarization introduced here [Eq. 5] goes beyond previous considerations because it accounts for the behaviour on the two halves of the system [46]. Here we will explore the nonlocal Majorana polarization \mathcal{P} , which will be obtained for an open chain in real space.

In what follows, we investigate the usefulness of the Majorana polarization \mathcal{P} to characterize the topological phase and detect the emergence of MZMs in the presence of TZESs. For this reason, we numerically obtain \mathcal{P} and \mathcal{M} in open and closed finite systems, respectively. Furthermore, we also discuss the energy spectra of the respective systems and contrast with the predictions of \mathcal{P} and \mathcal{M} . Throughout this work we consider realistic values such that $\Delta = 0.1t$, $\alpha = 0.1t$, which correspond to InAs nanowires and Al superconductors [47]. For completeness we provide analytic calculation of \mathcal{P} using minimal Kitaev chain in Appendix A.

III. SUPERCONDUCTING NANOWIRE

To begin, we analyze the topological properties of a superconducting nanowire modeled by Eq. (1) in the absence and presence of scalar disorder, characterized by $V(j)$. In this case, the pair potential (Δ) and chemical potential (μ) are homogeneous all over the nanowire. We explore the Pfaffian and Majorana polarization, which are obtained as discussed in Section II. Moreover, we also inspect the low-energy spectrum as it reveals the emergence of MZMs.

A. Superconducting nanowire without disorder

In the absence of disorder, $V(j) = 0$ in Eq. (1) and the calculation is carried out numerically. In Fig. 2(a) we present the Pfaffian invariant \mathcal{M} for a closed system as a function of the Zeeman field B and chemical potential μ , where the blue (red) region corresponds to the topological nontrivial (trivial) phase. The white region between the trivial and topological phases corresponds to the topological phase transition $B = B_c$. The green curve in Fig. 2(a) is the Majorana polarization \mathcal{P} obtained for an open system. In Fig. 2(b) and Fig. 2(c) we present the Zeeman dependent low-energy spectrum for a closed and an open system, respectively, which is accompanied by the Pfaffian \mathcal{M} and Majorana polarization \mathcal{P} .

The immediate feature we note in Fig. 2(a) is that the Pfaffian \mathcal{M} clearly identifies the trivial and topological phases as well as the topological phase transition between them, see red, blue, and white regions. The Pfaffian, however, signals the topological phase transition for a closed system. Notably, by looking at the Majorana polarization \mathcal{P} in the same panel, obtained for open boundary conditions, we observe that it directly probes the topological phase transition, agreeing perfectly well with the result predicted by the Pfaffian, see green curve between blue and red regions in Fig. 2(a). This suggests that \mathcal{P} can be also seen as a topological indicator. By inspecting the low-energy spectrum as a function of the Zeeman field at fixed chemical potential (white dashed line in panel (a)), we find that the Pfaffian obtained for a closed system indeed senses the topological phase transition, as depicted by the red curve jumping from $\mathcal{M} = 1$ to $\mathcal{M} = -1$ at $B = B_c$ in Fig. 2(b). Note that no MZMs are present in the closed system. In the case of the low-energy spectrum for the open system in Fig. 2(c), the Majorana polarization vanishes for $B < B_c$ but, interestingly, reaches $\mathcal{P} = -1$ at the topological phase transition and remains at such value all over the topological phase $B > B_c$ where MZMs appear. Thus, the Majorana polarization not only signals the topological phase transition but it also detects the presence of MZMs, supporting its interpretation as an alternative real space topological indicator.

The vanishing (finite) value of the Majorana polarization in the trivial (topological) phase seen in Fig. 2(c) can

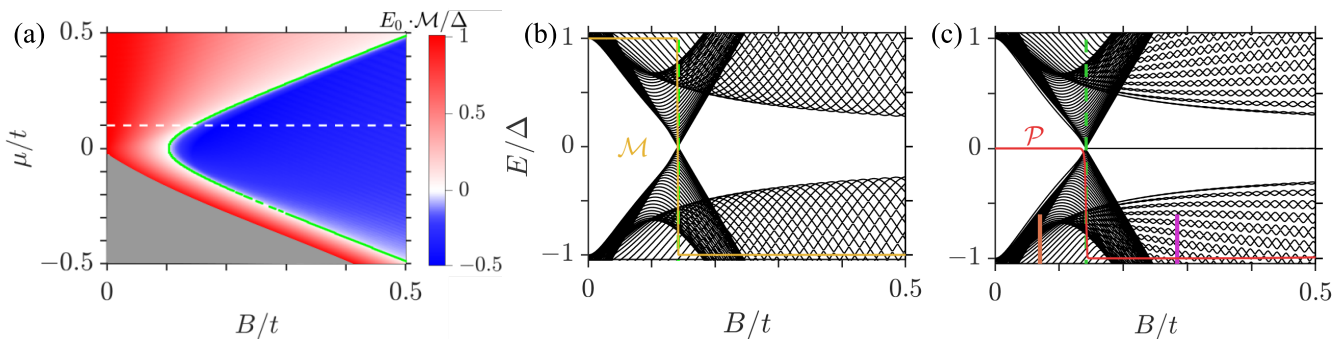


Figure 2. Topological phase and low-energy spectrum for a superconducting nanowire. (a) Pfaffian \mathcal{M} from Eq. (2) obtained for a closed system as a function of the chemical potential μ and Zeeman field B , with the intensity given by $E_0 \cdot \mathcal{M}/\Delta$, where E_0 corresponds to the lowest energy level. Here, the blue and red regions depict the nontrivial and trivial topological phases, respectively, while the white region indicates the phase transition. The grey region corresponds to $E_0/\Delta > 1$. The green curve in (a) corresponds to the topological phase transition line obtained from the Majorana polarization \mathcal{P} in an open system, showing great agreement with the Pfaffian predicted phase transition. (b) Low-energy spectrum and the Pfaffian \mathcal{M} (yellow curve) for a closed system as a function of the Zeeman field B at μ marked by the white dashed line in (a). (c) Same as (b) but for an open chain with $L = 300a$ and the Majorana polarization \mathcal{P} indicated by red curve. Note the absence (presence) of MZMs in panel (b) (panel (c)). Parameters: $\Delta/t = \alpha/t = 0.1$ and $\mu/t = 0.1$ in (b,c) indicated by dashed white line in (a).

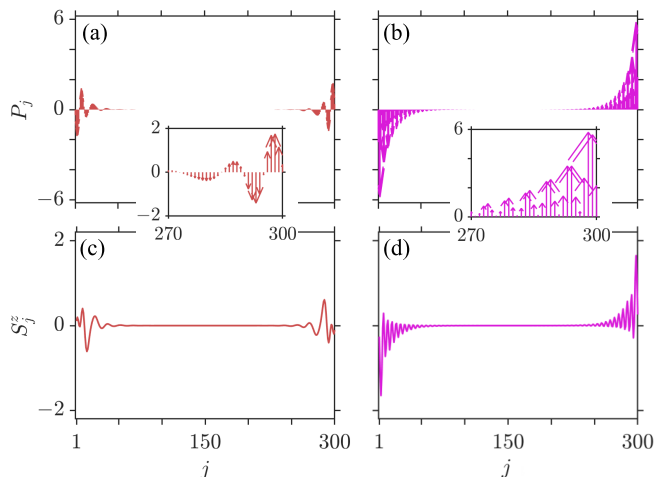


Figure 3. Spatial profiles of the onsite Majorana polarization from Eq. (3) (a,b) and the spin projection along z (b,d) in an open chain with $L = 300a$. The colors correspond to the color bars in Fig. 2(c). Insets in (a,b) show zoom-in at right edge. In all panels the vertical axes have been multiplied by 10^2 .

be understood by inspecting the real space dependence of the onsite Majorana polarization contributions, denoted by P_j in Eq. (3). In Fig. 3 we plot P_j as a function of space at Zeeman fields in the trivial and topological phase, indicated by orange and magenta bars in Fig. 2(c). In the trivial phase $B < B_c$, the onsite Majorana polarization P_j oscillates in space acquiring amplitudes that are opposite in sign, which, when summing them up to obtain the left and right Majorana polarizations $P_{L/R}$ in Eq. (4), give vanishing contribution for the Majorana polarization \mathcal{P} in Eq. (5). In contrast, in the topological phase $B > B_c$, the onsite Majorana polarization P_j develops large values at the edges and exhibits an oscillatory

decay with amplitudes having the same sign up to the middle of the system $L/2$: $P_j < 0$ for the left half, while $P_j > 0$ for the right half. Thus, when summing up P_j to find the left and right Majorana polarizations $P_{L/R}$ in Eq. (4), $P_{L/R}$ do not vanish, in contrast to what occurs in the trivial phase. As a result, the finite value of both P_L and P_R prevent the overall vanishing value of $\mathcal{P} = P_L P_R^* = P_L^* P_R$ in Eq. (5), which then explains why \mathcal{P} is finite in the topological phase. When normalizing it to the density-of states, we find $P_L = -1$ and $P_R = 1$, which gives $\mathcal{P} = -1$. Before closing this part, we point out that the behaviour of the Majorana polarization follows the corresponding profile of the spin projection, as we indeed observe in Fig. 3(c,d) for the spin density along z , obtained as $S^z = \Psi_j^\dagger \sigma_z \Psi_j$, where Ψ_j is the wavefunction associated to the lowest energy state. Of particular interest is that the onsite Majorana polarization follows the same sign of the spin projection, revealing that the negative sign of \mathcal{P} has natural physical interpretation. In sum, the Majorana polarization is not only a good real space topological indicator that signals the topological phase transition but it can also be used to identify the formation of MZMs and their spatial overlap.

B. Superconducting nanowire with disorder

Having shown the potential of the Majorana polarization to characterize the topological phase and the emergence of MZMs in the previous section, here we explore its robustness under the presence of scalar disorder. The choice of this type of disorder is motivated by the fact that it is very likely to be present in realistic superconductor-semiconductor systems [18, 48–50], see also Refs. [34, 51]. To model scalar disorder, we consider random site-dependent fluctuations characterized by the

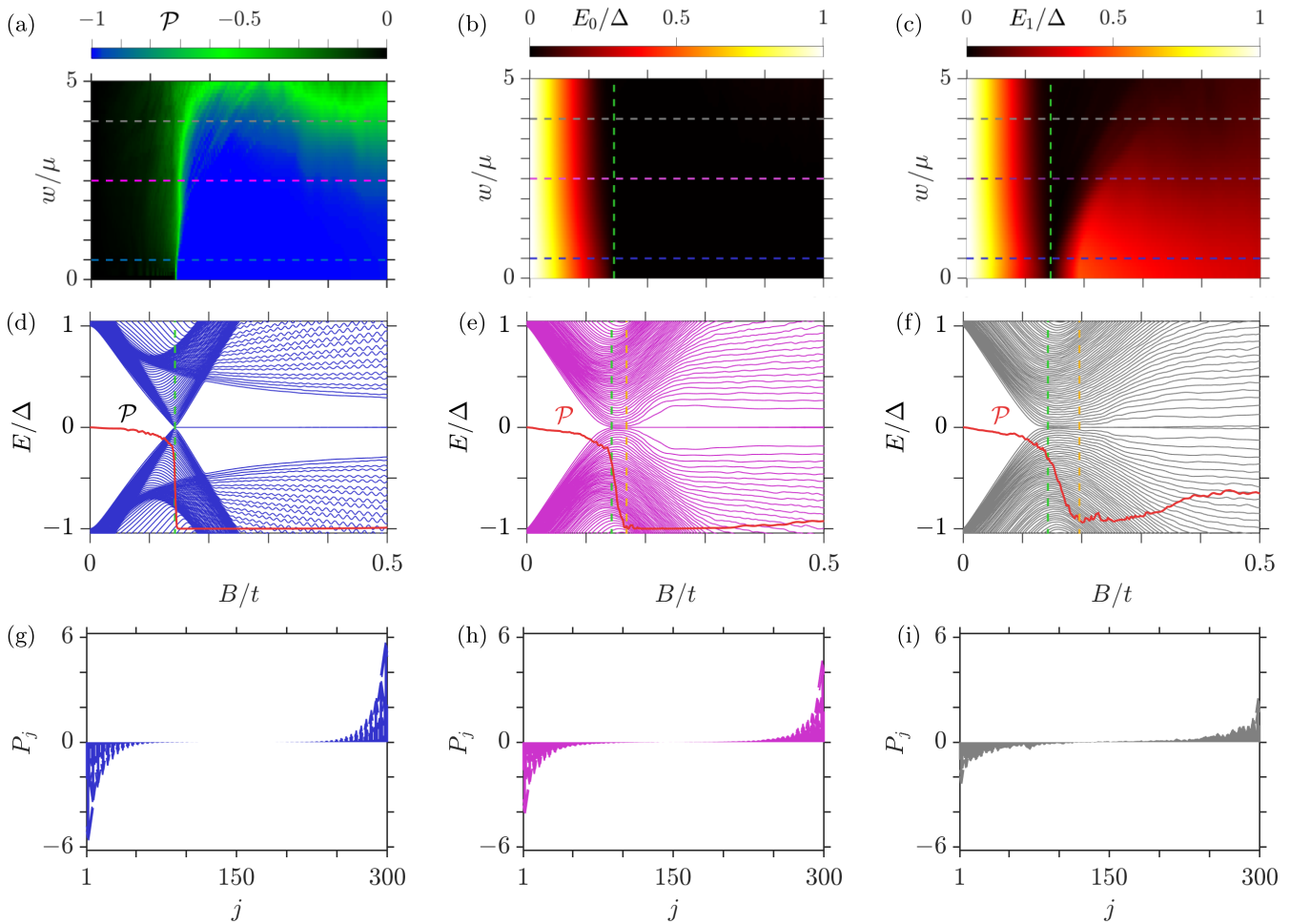


Figure 4. Phase diagram and low-energy spectrum for an open superconducting nanowire under scalar disorder, averaged over 40 disorder configurations. (a) Majorana polarization \mathcal{P} as a function of the Zeeman field and disorder strength w at $\mu/t = 0.1$ (white dashed line in Fig. 2(a)). Panels (b,c) show the lowest and first excited energy levels $E_{0,1}$ as a function of B and w at $\mu/t = 0.1$, as in (a). The vertical green dashed line marks the topological phase transition in the absence of disorder. (d-f) Low-energy spectrum as a function of B at three distinct values of disorder, which correspond to the weak (d) and strong disorder regimes (e,f), marked by dashed lines in (a-c) with corresponding colors. The Majorana polarization in (d-f) is shown by the red curve. In (d-f), the yellow line marks the topological transition point in the presence of disorder. (g-i) Onsite Majorana polarization P_j in the topological phase at $B = 2B_c$ in (d-f) with corresponding colors. The vertical axes of (g-i) have been multiplied by 10^2 . The rest of parameters are the same as the used in Fig. 3. For these parameters strong disorder is obtained when $w/\mu \gtrsim 1.5$.

potential $V(j)$ in Eq. (1),

$$V(j) = \sum_{j\sigma} d_{j\sigma}^\dagger [\delta\mu(j)] d_{j\sigma} + \text{H.c.}, \quad (6)$$

where $\delta\mu(j) \in [-w, w]$ describes site-dependent random fluctuations with w denoting the disorder strength, which ensures that $\langle \delta\mu \rangle = 0$. To characterize the amount of disorder, we compare the amplitude of the fluctuations with respect to the chemical potential, w/μ , since $V(j)$ can be seen as fluctuations around μ . Then, as in the previous section, we numerically calculate the Majorana polarization and the low-energy spectrum including $V(j)$ from Eq. (6) into the superconducting nanowire Hamiltonian given by Eq. (1).

In Fig. 4(a-c) we plot the disorder-averaged of the Majorana polarization \mathcal{P} and the lowest and first excited energy levels $E_{0,1}$ as a function of the Zeeman field B and disorder strength w at fixed chemical potential. In Fig. 4(d-f) we plot the low-energy spectrum and \mathcal{P} as a function of B as three distinct disorder strengths, while in Fig. 4(g-i) the corresponding onsite P_j Majorana polarization as a function of space in the topological phase $B = 2B_c$. For the chosen parameters, strong disorder is achieved when $w/\mu \gtrsim 1.5$, indicating that (d) is already in the weak-to-intermediate disorder regime, while (e,f) in the strong disorder regime. The first feature to notice is that \mathcal{P} vanishes in the trivial phase for weak-to-intermediate strengths of disorder, develop a sharp tran-

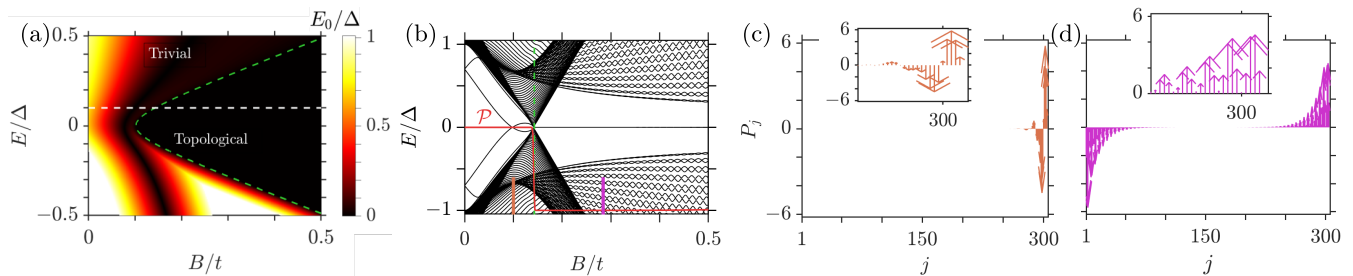


Figure 5. Low-energy spectrum and Majorana polarization in NS junctions. (a) Lowest energy level E_0 as a function of the Zeeman field B and chemical potential in the S region μ_S at $\mu_N = 0.1t$. The dashed green curve corresponds to the topological phase obtained from the Majorana polarization \mathcal{P} for an homogeneous superconductor. (b) Low-energy spectrum and Majorana polarization \mathcal{P} (red curve) as function of B at $\mu_{S,N} = 0.1t$ marked by the dashed white line in (a). (c,d) Onsite Majorana polarization P_j as a function of space at fixed Zeeman fields in the trivial and topological phases, marked by blue and red bars in (b). The vertical axes of (c,d) have been multiplied by 10^2 . Parameters: $L_N = 4a$, $L_S = 300a$. Rest of parameters are the same as in Fig. 4.

sition at the topological phase transition, and acquires a finite value and equal to -1 in the topological phase, see black and brightest regions below dashed blue curve in Fig. 4(a). The behavior of \mathcal{P} reflects the formation of MZMs and the gap closing and reopening in Fig. 4(b,c). At intermediate values of disorder, \mathcal{P} still remains a good indicator, with roughly vanishing values below B_c and equal to -1 in the topological phase, see dashed blue curve in Fig. 4(a) and also Fig. 4(d). At strong disorder, \mathcal{P} surprisingly still captures well the topological phase transition even when the visibility of the gap closing and reopening is considerably degraded by an avalanche of TZESs around $B = B_c$, see black/dark and bright regions below magenta line in Fig. 4(a-c) and also Fig. 4(d). In fact, $\mathcal{P} \approx -1$ after the topological phase transition (yellow dashed line) in Fig. 4(e), revealing the emergence of well-localized MZMs. This behavior roughly remains at larger values of disorder, with \mathcal{P} being very small below B_c but large in the topological phase, see Fig. 4(a-c). It is worth noting, however, that the Majorana polarization at very strong disorder in the topological phase ultimately deviates from -1 because MZMs acquire a finite spatial overlap that leads to finite energies, see Fig. 4(f).

As in the case without disorder, the finite value of the Majorana polarization \mathcal{P} in the presence of disorder originates from the individual contributions of P_j in Eq. (3). In fact, in the topological phase, the left and right Majorana polarizations that determine \mathcal{P} develop large values at the edges of the system and decay with an oscillatory fashion towards the bulk of the system, see Fig. 4(g-i). Interestingly, the oscillations of the left (right) Majorana polarization exhibit the same sign, which then lead to a finite value of \mathcal{P} in the topological phase. We note that it is the amplitude of P_j that gets degraded with the increase of disorder but the spatial profile remains the same. We can therefore conclude that the Majorana polarization \mathcal{P} , as defined in Eq. (5), represents a good topological indicator to characterize the topological phase transition and the emergence of MZMs even in

the presence of strong disorder when TZESs appear.

For completeness in Appendix B we present the results for single disorder realization and compare \mathcal{P} and \mathcal{M} . The results show the \mathcal{M} fails to capture the topological phase in the presence of TZESs while \mathcal{P} proof to be a robust topological indicator.

IV. SN JUNCTIONS WITH TRIVIAL ZERO-ENERGY STATES

Up to here, we have discussed the Majorana polarization as a tool to characterize the topological phase and MZMs in single superconducting wires even when disorder-induced TZESs appear. In this part, we consider SN junctions with SOC under a Zeeman field and investigate the potential of the Majorana polarization to distinguish between MZMs and TZESs. We remark that SN junctions represent another experimentally relevant platform where TZESs emerge due to confinement effects of the N region [14, 15, 19]. Thus, we take the model given by Eq. (1) and set $\Delta = 0$ in N with chemical potential μ_N and length L_N , while S has $\Delta \neq 0$ with chemical potential μ_S and length L_S . Then, we obtain the Majorana polarization and low-energy spectrum as discussed in Section II; see also previous Section III. In Fig. 5(a) we plot the lowest energy level E_0 as a function of the Zeeman field B and chemical potential in the S region μ_S for a short N region with $\mu_N = 0.1t$ and relatively long S region. Therein, the dashed green curve marks the topological phase transition obtained from the Majorana polarization \mathcal{P} . Fig. 5(b) shows the low-energy spectrum and Majorana polarization as a function of B at $\mu_{N(S)} = 0.1t$, while Fig. 5(c,d) show the onsite Majorana polarization P_j at Zeeman fields that originate MZMs and TZESs Fig. 5(b).

The first of observation in Fig. 5(a) is that E_0 reaches zero well before the topological phase transition, which signals the emergence of a TZES whose energy, however,

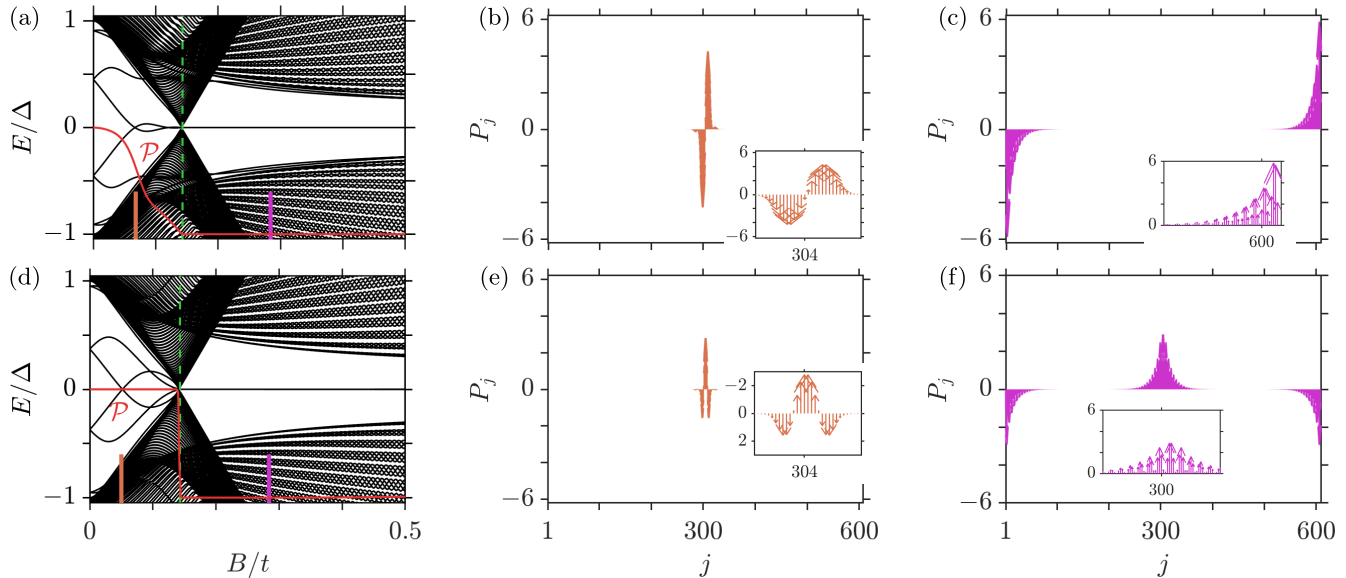


Figure 6. (a,d) Low-energy spectrum and Majorana polarization in red color as a function of the Zeeman field B for a short SNS Josephson junction at $\phi = 0$ and $\phi = \pi$. Panels (b,c) show the real space dependence of the onsite Majorana polarization P_j for $\phi = 0$ at Zeeman fields in the trivial and topological phases, marked by blue and red vertical lines in (a). Panels (e,f) show the same as (b,c) but at $\phi = \pi$. The vertical axes of (b,c,e,f) have been multiplied by 10^2 . Parameters: $\mu_N = 0$, $\mu_S = 0.1t$, $L_N = 8a$, $L_S = 300a$, and the rest of parameters considered as in Fig. 2.

strongly depends on the chemical potential μ_S . The formation of the TZES can be also seen in the full low-energy in Fig. 5(b), where a single level crossing appears below B_c (green dashed line) for the chosen parameters. We have verified that this TZES is located at the interface between the S and N regions, with no counterpart at the leftmost side of S, as expected for a trivial bound state. This TZES here appears due to confinement in the finite N region and is thus very sensitive to the choice of parameters [19, 22]. More TZESs can form when taking longer N regions. The second observation is that the Majorana polarization, indicated by the red curve in Fig. 5(b), vanishes $\mathcal{P} = 0$ all over the trivial phase even at Zeeman fields where the TZES appears. Remarkably, the Majorana polarization jumps to $\mathcal{P} = -1$ at the topological phase transition (green dashed line) and remains unity all over the topological phase, signalling the emergence of truly MZMs. The vanishing value of \mathcal{P} in the trivial phase is a result of the onsite Majorana polarization P_j acquiring opposite signs in the right half of the wire, which here occurs even in the presence of TZESs induced by confinement, see Fig. 5(c); the left half exhibits vanishing P_j because there is no bound state on that side; the TZES here localizes at the interface between the right side of S and N. Remarkably, in the topological phase, the onsite Majorana polarization P_j for the left and right halves decay with an exponentially oscillatory profile that do not change the sign of their amplitudes, resulting in a finite value of $P_{L/R}$ when summing up P_j in the left/right halves. Thus, the origin of the finite (vanishing) Majorana polarization in the topological (trivial)

phases is the same as the one discussed in the previous two sections. We can therefore conclude that the Majorana polarization also distinguishes between MZMs and TZESs in NS junctions.

V. SNS JUNCTIONS WITH FOUR MAJORANA ZERO MODES

To further demonstrate the utility of the Majorana polarization, here we employ it to characterize the topological phase in short SNS Josephson junctions, where the length of the N region is shorter than the superconducting coherence length. As explained in Section II, we assume that N has zero pair potential $\Delta = 0$, chemical potential μ_N , and length L_N , while the S regions have pair potential $\Delta \neq 0$, chemical potential μ_S , and length L_S . We also consider that there is a finite phase difference between the pair potentials of the superconductors, denoted here by ϕ . Before we go further, we note that these type of Josephson junctions host two MZMs at $\phi = 0$ located at the outer ends of the junction, while four MZMs at $\phi = \pi$, two located at the outer sides and two at the inner sides of the SNS junction, see Fig. 1(c,d) and also Refs. [52–54]. For this reason, we focus on $\phi = 0, \pi$ and analyze the Majorana polarization \mathcal{P} for signalling the formation of MZMs. Since $\phi = 0$ and $\phi = \pi$ correspond to a distinct number of MZMs located at different positions, see above, the calculation of \mathcal{P} depends on $\phi = 0$. In particular, at $\phi = 0$, the Majorana polarization \mathcal{P} is carried out by dividing the total system into two parts,

which serve to calculate the left and right Majorana polarizations $P_{L/R}$ according to Eq. (4). So, the site index j in Eq. (4) here runs up to the middle of the N region. In contrast, at $\phi = \pi$, we obtain \mathcal{P} by taking only half of the total junction, which is then divided into two parts that then are used to find $P_{L/R}$ according to Eq. (4). We carried out this step because using the full system at $\phi = \pi$ will lead to double counting and hence vanishing values of Majorana polarization in the presence of the four MZMs. With these annotations, we calculate \mathcal{P} at $\phi = 0, \pi$.

In Fig. 6(a,d) we show the low-energy spectrum and Majorana polarization \mathcal{P} as a function of the Zeeman field B at $\phi = 0, \pi$ for a short N region with $L_N = 8a$ and sufficiently long S regions $L_S = 300a$. Moreover, Fig. 6(b,c) and Fig. 6(e,f) depict the spatial dependence of the onsite Majorana polarization P_j at $\phi = 0$ and $\phi = \pi$, respectively, for two Zeeman fields in the trivial and topological phases, marked by blue and red bars in (a). We first note that, for the chosen parameters, the system hosts TZESs below the topological phase transition marked by the green dashed line, see Fig. 6(a,d). The TZESs at $\phi = 0$ have the same origin as those found in the case of NS junctions and presented in Fig. 5(b). The TZESs at $\phi = \pi$, however, have a distinct origin because they entirely dependent on the phase difference ϕ , which also makes them easily tunable away from zero energy [22]. Nevertheless, these TZESs might also occur in realistic superconductor-semiconductor systems, which is the motivation for the choice of parameters in Fig. 6. In the topological phase, the low-energy spectrum reveals the emergence of MZMs at $\phi = 0$ and $\phi = \pi$, as expected [52–54]. When inspecting the Majorana polarization \mathcal{P} , at $\phi = 0$ we observe that it has vanishing values at very small B but smoothly increases up to the topological phase transition but always below -1 , see red curve in Fig. 6(a); note that \mathcal{P} does not remain constant in the trivial phase even with TZESs as a result of the spatial dependence of P_j , see below. At $\phi = \pi$, the Majorana polarization vanishes all over the trivial phase even in the presence of TZESs originating from P_j , see red curve in Fig. 6(d). Notably, at the topological phase transition (green dashed line), the Majorana polarization jumps to $\mathcal{P} = -1$ and remains at such value in the entire topological as B increases, an effect occurring in the presence of two MZMs at $\phi = 0$ and also in the presence of four MZMs at $\phi = \pi$, see red curves in Fig. 6(a,d). The fact that the Majorana polarization becomes $\mathcal{P} = -1$ is a strong indicator of the emergence of truly MZMs, which here we show to occur also for MZMs in Josephson junctions.

The finite values of the Majorana polarization \mathcal{P} in the trivial phase at $\phi = 0$ can be understood by noting that $P_{L/R}$, which then determine \mathcal{P} as given by Eq. (5), are obtained by summing up P_j in the left/right half of the total system (the SNS junction). Here, P_j has finite values at the junction with opposite signs because of the localization of a TZES. As we see in Fig. 6(b), the left (right) half has finite P_j with the same sign and there-

fore do not cancel out when summing them up to obtain $P_{L/R}$ and then producing a finite \mathcal{P} . This effect does not occur at $\phi = \pi$ in the trivial phase [Fig. 6(a)] because, being the taken system only the left superconductor and the TZES located at the junction, implies that P_j has vanishing values in the left half of the left superconductor. Hence, $P_L = 0$ and $\mathcal{P} = 0$ at $\phi = \pi$ in the trivial phase. In the topological phase, P_j reveals intriguing features about MZMs. At $\phi = 0$, the outer MZMs exhibit P_j with opposite signs but this situation changes at $\phi = \pi$, where P_j for the outer MZMs acquires the same sign. This happens due to the emergence of two extra MZMs at the inner sides of the junction, which exhibit P_j of the same sign. Thus, the opposite sign profile of P_j in each S region is still preserved, with $\mathcal{P} = -1$, in agreement to what we have discussed in previous sections for the single superconducting wire and NS junctions.

VI. CONCLUDING REMARKS

In conclusion, we have investigated the Majorana polarization for distinguishing between Majorana and trivial zero-energy states in superconducting systems with spin-orbit coupling and Zeeman field. In particular, we have studied superconducting nanowires with and without disorder, NS junctions, and SNS junctions. We have shown that the Majorana polarization represents a robust real space topological invariant that is able to detect not only the topological phase transition but also reveals the spatial nonlocality of Majorana zero modes. Interestingly, we have demonstrated that the Majorana polarization is robust against strong scalar disorder and serves as an alternative tool to distinguish between Majorana and trivial zero-energy states.

The nonlocal Majorana polarization investigated here also leaves open questions. For instance, the fact that the Majorana polarization is able to identify the topological phase transition and the formation of Majorana zero modes suggests that it captures properties of the emergent topological superconducting state. As such, there seems to be an intriguing relation between Majorana polarization and emergent superconductivity, which might also require to generalize the definition adopted here to the many-body realm [55] and therefore deserves further investigation. Another interesting problem is about the measurement of the Majorana polarization. To access the Majorana polarization, it is necessary to obtain the coherence factors u and v , see Eq. (3). One possible approach to measure such coherence factors is through Andreev spectroscopy [56], which can be complemented by measurements of the local density of states measurements [57]. Although this task is nontrivial, detecting the Majorana polarization would help characterizing the nature of zero-energy states in Majorana devices.

ACKNOWLEDGMENTS

We thank M. Leijnse for important comments on the manuscript. O. A. A. acknowledges funding from NanoLund, the Swedish Research Council (Grant Agreement No. 2020-03412) and the European Research Council (ERC) under the European Union's Horizon 2020 research and innovation programme under the Grant Agreement No. 856526. The computations were enabled by resources provided by the National Academic Infrastructure for Supercomputing in Sweden (NAISS) and the Swedish National Infrastructure for Computing (SNIC) at UPPMAX partially funded by the Swedish Research Council (Grant Agreement No. 2020-03412). J. C. acknowledges financial support from the Swedish Research Council (Vetenskapsrådet Grant No. 2021-04121) and the Carl Trygger's Foundation (Grant No. 22: 2093).

Appendix A: Majorana polarization in a two-site Kitaev chain

In this part we analyze the Majorana polarization in a minimal Kitaev chain consisting of two spin-polarized sites with p -wave pairing [58]

$$H_{2\text{KC}} = \sum_{\alpha=L,R} \varepsilon_{\alpha} d_{\alpha}^{\dagger} d_{\alpha} + t d_{L}^{\dagger} d_{R} + \Delta d_{L}^{\dagger} d_{R}^{\dagger} + \text{H.c.} \quad (\text{A1})$$

where L and R label the two (left and right) sites, ε_{α} is the onsite energy of site $\alpha = L, R$, t is the hopping amplitude, and Δ the p -wave pair potential. The two-site Kitaev chain described by Eq. (A1), despite its evident simplicity, holds experimental relevance because it has been recently realized using superconductor-semiconductor systems [59]. Majorana states in Eq. (A1) emerge at the so called sweet spot when $\varepsilon_{L,R} = 0$ and $\Delta = t$, see Ref. [58]. To see the emergence of Majorana states, we write Eq. (A1) in Nambu basis with $\psi = (d_L, d_R, d_L^{\dagger}, d_R^{\dagger})^T$ and find the eigenvalues and eigenvectors. Then, the lowest energies in the sweet spot are $E_{\pm}^0 = 0$, and their associated normalized eigenvectors are given by

$$\begin{aligned} \Psi_{E_+^0} &= \frac{1}{\sqrt{2}}(0, 1, 0, 1)^T, \\ \Psi_{E_-^0} &= \frac{1}{\sqrt{2}}(-1, 0, 1, 0)^T. \end{aligned} \quad (\text{A2})$$

By a simple inspection, and reminding the structure of the basis vector ψ , we notice that $\Psi_{E_+^0}$ is located in the right site $\alpha = R$, while $\Psi_{E_-^0}$ is located in the left site $\alpha = L$. Hence, the lowest states of the two-site Kitaev chain in the sweet spot exhibit zero energy and are non-local. Moreover, $\gamma_{L/R} = \psi \cdot \Psi_{L,R} = \gamma_{L/R}^{\dagger}$ and therefore defines a Majorana operator. These properties allowed to interpret the states defined by Eq. (A2) as Majorana

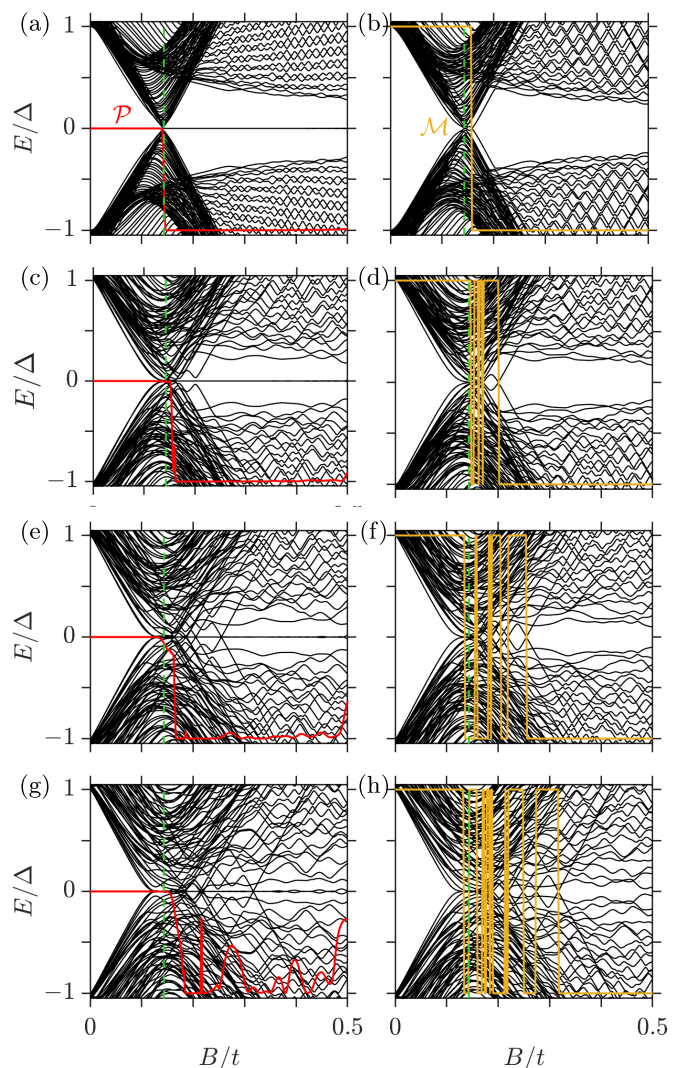


Figure A1. Low energy spectrum, Majorana polarization, \mathcal{M} (left) and Pfaffian, \mathcal{M} (right), for a single disorder realization as functions of Zeeman field, B for several disorder strength values (a,b) $w/\mu = 1$, (c,d) $w/\mu = 2$, (e,f) $w/\mu = 3$, and (g,h) $w/\mu = 4$.

quasiparticles; since there is no topological protection, they are called poor man's Majorana modes [58].

Here we are interested in exploring the expectation value of the particle-hole operator, a quantity identified before as Majorana polarization. In the considered basis, the particle-hole operator is given by $\mathcal{C} = \tau^x$, where τ_i is i -th Pauli matrix in Nambu subspace. Then, the expectation value of the particle-hole operator \mathcal{C} , or Majorana polarization, for each wavefunction in Eq. (A2) is given by

$$\begin{aligned} p_L &= \langle \Psi_{E_+^0} | \mathcal{C} | \Psi_{E_+^0} \rangle = -1, \\ p_R &= \langle \Psi_{E_-^0} | \mathcal{C} | \Psi_{E_-^0} \rangle = 1, \end{aligned} \quad (\text{A3})$$

where we have used the subscript L/R because $\Psi_{E_{+/-}^0}$ are located in the left/right site. At this point we remark

that the left and right Majorana state exhibit a Majorana polarization with opposite sign. Then, by defining a nonlocal Majorana polarization as $p = p_L^* \cdot p_R = p_L \cdot p_R^*$, it is natural to interpret that $p = -1$ provides information about the existence of both Majorana-like states perfectly localized in the left and right sites of the two-site Kitaev model given by Eq. (A1) in the sweet spot. Although there is no exponential protection, no topological number, the total Majorana polarization is able to identify the formation of the two MZMs. For obvious reasons, these MZMs have been coined poor man's Majorana modes [58].

Away from the sweet spot, when $\varepsilon_{L/R} = \varepsilon$ and $\Delta \neq t$, the Majorana polarizations become $p_L = -p_R = \Delta/\sqrt{\Delta^2 + \varepsilon^2}$, which then leads to $p = p_L \cdot p_R \approx -1 + 2(\varepsilon/\Delta)^2$ for $\varepsilon \ll \Delta$. Hence, as ε moves away from zero acquiring finite values, the nonlocal Majorana polarization becomes $p > -1$ signaling that MZMs hybridize. For $\varepsilon \gg \Delta$, the Majorana polarization reads $p \approx -(\Delta/\varepsilon)^2$, which practically becomes a very small number, again signalling a strong Majorana hybridization. In the general case, $\varepsilon_L \neq \varepsilon_R$, MZMs are challenging to realize and the nonlocal Majorana polarization p takes a convoluted form.

Appendix B: Comparison between the Pfaffian and Majorana polarization in disordered systems

In the main text we presented disorder-averaged spectrum and showed that the Majorana polarization, \mathcal{P} , captures the topological phase accurately, albeit for very strong disorder it deviates from unity due to strong cor-

relation between the MZMs s expected. We also mentioned that the \mathcal{M} fails to distinguish between MZMs and TZESs: due to the fact that \mathcal{M} captures changes in the fermion parity of the ground state. Hence, \mathcal{M} changes for any zero-energy crossing, trivial or nontrivial.

In this Appendix, we compare \mathcal{P} and \mathcal{M} in the presence of plethora TZESs induced by disorder. Fig. A1(a,c,e,g) shows the low energy spectrum for open chain (black) and \mathcal{P} (red) while Fig. A1(b,d,f,h) shows the low energy spectrum for closed (black) and \mathcal{M} (gold) for single disorder realization several disorder strength values. At weak disorder (a,b), both \mathcal{P} and \mathcal{M} accurately captures the topological transition. At intermediate, \mathcal{P} (c) still captures the topological phases accurately despite the presence of disorder-induced TZESs while \mathcal{M} (d) changes at every zero-energy crossing. Thus, \mathcal{P} is a good topological indicator in the presence TZESs. The reason for this is that \mathcal{P} only takes into account the MZMs and the correlation between them. Thus, as long as the perturbation does not induce a large cross-talk between the MZMs \mathcal{P} is robust. On the other hand, \mathcal{M} is a bulk quantity as such any changes in fermion parity changes it rendering it a poor topological indicator for inhomogeneous systems. Further increasing the disorder strength \mathcal{P} (e,g) deviates from -1 indicating that the topological phase is being destroyed by disorder while the fluctuation in \mathcal{M} increases as the number of zero-energy crossing of trivial states increase with disorder strength (f,h).

Thus, from these results we conclude that \mathcal{P} remains a good topological indicator under the presence of TZESs, thus revealing its potential as a useful tool for the analysis of MZMs in realistic systems.

-
- [1] M. Leijnse and K. Flensberg, Introduction to topological superconductivity and majorana fermions, *Semicond. Sci. Technol.* **27**, 124003 (2012).
 - [2] M. Sato and S. Fujimoto, Majorana fermions and topology in superconductors, *J. Phys. Soc. Jpn.* **85**, 072001 (2016).
 - [3] M. Sato and Y. Ando, Topological superconductors: a review, *Reports on Progress in Physics* **80**, 076501 (2017).
 - [4] R. Aguado, Majorana quasiparticles in condensed matter, *Riv. Nuovo Cimento* **40**, 523 (2017).
 - [5] Y. Tanaka, M. Sato, and N. Nagaosa, Symmetry and topology in superconductors –odd-frequency pairing and edge states–, *J. Phys. Soc. Jpn* **81**, 011013 (2012).
 - [6] S. M. Frolov, M. J. Manfra, and J. D. Sau, Topological superconductivity in hybrid devices, *Nat. Phys.* **16**, 718 (2020).
 - [7] K. Flensberg, F. von Oppen, and A. Stern, Engineered platforms for topological superconductivity and Majorana zero modes, *Nat. Rev. Mater.* **6**, 944 (2021).
 - [8] A. Barman Ray, J. D. Sau, and I. Mandal, Symmetry-breaking signatures of multiple majorana zero modes in one-dimensional spin-triplet superconductors, *Phys. Rev. B* **104**, 104513 (2021).
 - [9] P. Marra, Majorana nanowires for topological quantum computation, *J. Appl. Phys.* **132**, 231101 (2022).
 - [10] Y. Tanaka, S. Tamura, and J. Cayao, Theory of Majorana zero modes in unconventional superconductors, arXiv:2402.00643 (2024).
 - [11] E. Prada, P. San-Jose, M. W. de Moor, A. Geresdi, E. J. Lee, J. Klinovaja, D. Loss, J. Nygård, R. Aguado, and L. P. Kouwenhoven, From Andreev to Majorana bound states in hybrid superconductor–semiconductor nanowires, *Nat. Rev. Phys.* **2**, 575 (2020).
 - [12] D. Bagrets and A. Altland, Class *D* spectral peak in Majorana quantum wires, *Phys. Rev. Lett.* **109**, 227005 (2012).
 - [13] D. I. Pikulin, J. P. Dahlhaus, M. Wimmer, H. Schomeerus, and C. W. J. Beenakker, A zero-voltage conductance peak from weak antilocalization in a Majorana nanowire, *New J. Phys.* **14**, 125011 (2012).
 - [14] G. Kells, D. Meidan, and P. W. Brouwer, Near-zero-energy end states in topologically trivial spin-orbit coupled superconducting nanowires with a smooth confinement, *Phys. Rev. B* **86**, 100503 (2012).
 - [15] J. Cayao, E. Prada, P. San-Jose, and R. Aguado, Sns junctions in nanowires with spin-orbit coupling: Role of

- confinement and helicity on the subgap spectrum, *Phys. Rev. B* **91**, 024514 (2015).
- [16] E. Prada, P. San-Jose, and R. Aguado, Transport spectroscopy of NS nanowire junctions with Majorana fermions, *Phys. Rev. B* **86**, 180503 (2012).
- [17] C. Reeg, O. Dmytruk, D. Chevallerier, D. Loss, and J. Klinovaja, Zero-energy Andreev bound states from quantum dots in proximitized Rashba nanowires, *Phys. Rev. B* **98**, 245407 (2018).
- [18] S. Das Sarma and H. Pan, Disorder-induced zero-bias peaks in Majorana nanowires, *Phys. Rev. B* **103**, 195158 (2021).
- [19] J. Cayao and P. Buset, Confinement-induced zero-bias peaks in conventional superconductor hybrids, *Phys. Rev. B* **104**, 134507 (2021).
- [20] O. A. Awoga, J. Cayao, and A. M. Black-Schaffer, Robust topological superconductivity in weakly coupled nanowire-superconductor hybrid structures, *Phys. Rev. B* **105**, 144509 (2022).
- [21] B. S. de Mendonça, A. L. R. Manesco, N. Sandler, and L. G. G. V. Dias da Silva, Near zero energy Caroli-de Gennes–Matricon vortex states in the presence of impurities, *Phys. Rev. B* **107**, 184509 (2023).
- [22] L. Baldo, L. G. G. V. Dias Da Silva, A. M. Black-Schaffer, and J. Cayao, Zero-frequency supercurrent susceptibility signatures of trivial and topological zero-energy states in nanowire junctions, *Supercond. Sci. Technol.* **36**, 034003 (2023).
- [23] O. A. Awoga, M. Leijnse, A. M. Black-Schaffer, and J. Cayao, Mitigating disorder-induced zero-energy states in weakly coupled superconductor-semiconductor hybrid systems, *Phys. Rev. B* **107**, 184519 (2023).
- [24] S. Pal and C. Benjamin, Honing in on a topological zero-bias conductance peak, *J. Phys: Condens. Matter* **36**, 035601 (2023).
- [25] Y. Tanaka and S. Kashiwaya, Theory of tunneling spectroscopy of *d*-wave superconductors, *Phys. Rev. Lett.* **74**, 3451 (1995).
- [26] S. Kashiwaya, Y. Tanaka, M. Koyanagi, and K. Kajimura, Theory for tunneling spectroscopy of anisotropic superconductors, *Phys. Rev. B* **53**, 2667 (1996).
- [27] S. Kashiwaya and Y. Tanaka, Tunneling effects on surface bound states in unconventional superconductors, *Rep. Prog. Phys.* **63**, 1641 (2000).
- [28] C. J. Bolech and E. Demler, Observing Majorana bound states in *p*-wave superconductors using noise measurements in tunneling experiments, *Phys. Rev. Lett.* **98**, 237002 (2007).
- [29] K. T. Law, P. A. Lee, and T. K. Ng, Majorana fermion induced resonant Andreev reflection, *Phys. Rev. Lett.* **103**, 237001 (2009).
- [30] K. Flensberg, Tunneling characteristics of a chain of Majorana bound states, *Phys. Rev. B* **82**, 180516 (2010).
- [31] M. Hell, K. Flensberg, and M. Leijnse, Distinguishing Majorana bound states from localized Andreev bound states by interferometry, *Phys. Rev. B* **97**, 161401 (2018).
- [32] O. A. Awoga, J. Cayao, and A. M. Black-Schaffer, Supercurrent detection of topologically trivial zero-energy states in nanowire junctions, *Phys. Rev. Lett.* **123**, 117001 (2019).
- [33] J. Cayao and A. M. Black-Schaffer, Distinguishing trivial and topological zero-energy states in long nanowire junctions, *Phys. Rev. B* **104**, L020501 (2021).
- [34] M. Aghaee, A. Akkala, Z. Alam, R. Ali, A. Alcaraz Ramirez, M. Andrzejczuk, A. E. Antipov, P. Aseev, M. Astafev, B. Bauer, J. Becker, S. Boddapati, F. Boekhout, J. Bommer, T. Bosma, L. Bourdet, S. Boutin, P. Caroff, L. Casparis, M. Cassidy, S. Chatterjee, A. W. Christensen, N. Clay, W. S. Cole, F. Corsetti, A. Cui, P. Dalampiras, A. Dokania, G. de Lange, M. de Moor, J. C. Estrada Saldaña, S. Fallahi, Z. H. Fathabad, J. Gamble, G. Gardner, D. Govender, F. Grigorio, R. Grigoryan, S. Gronin, J. Gukelberger, E. B. Hansen, S. Heedt, J. Herranz Zamorano, S. Ho, U. L. Holgaard, H. Ingerslev, L. Johansson, J. Jones, R. Kallagher, F. Karimi, T. Karzig, E. King, M. E. Kloster, C. Knapp, D. Kocon, J. Koski, P. Kostamo, P. Krogstrup, M. Kumar, T. Laeven, T. Larsen, K. Li, T. Lindemann, J. Love, R. Lutchny, M. H. Madsen, M. Manfra, S. Markussen, E. Martinez, R. McNeil, E. Memisevic, T. Morgan, A. Mullally, C. Nayak, J. Nielsen, W. H. P. Nielsen, B. Nijholt, A. Nurmohamed, E. O’Farrell, K. Otani, S. Pauka, K. Petersson, L. Petit, D. I. Pikulin, F. Preiss, M. Quintero-Perez, M. Rajpalke, K. Rasmussen, D. Razmadze, O. Reentila, D. Reilly, R. Rouse, I. Sadovskyy, L. Sainiemi, S. Schreppler, V. Sidorkin, A. Singh, S. Singh, S. Sinha, P. Sohr, T. c. v. Stankevič, L. Stek, H. Suominen, J. Suter, V. Svidenko, S. Teicher, M. Temuerhan, N. Thiyagarajah, R. Tholapi, M. Thomas, E. Toomey, S. Upadhyay, I. Urban, S. Vaitiekėnas, K. Van Hoogdalem, D. Van Woerkom, D. V. Viazmitinov, D. Vogel, S. Waddy, J. Watson, J. Weston, G. W. Winkler, C. K. Yang, S. Yau, D. Yi, E. Yucelen, A. Webster, R. Zeisel, and R. Zhao (Microsoft Quantum), InAs-Al hybrid devices passing the topological gap protocol, *Phys. Rev. B* **107**, 245423 (2023).
- [35] V. K. Vimal and J. Cayao, Entanglement measures of Majorana bound states, arXiv:2404.14900 (2024).
- [36] D. Sticlet, C. Bena, and P. Simon, Spin and Majorana polarization in topological superconducting wires, *Phys. Rev. Lett.* **108**, 096802 (2012).
- [37] N. Sedlmayr and C. Bena, Visualizing Majorana bound states in one and two dimensions using the generalized Majorana polarization, *Phys. Rev. B* **92**, 115115 (2015).
- [38] N. Sedlmayr, J. M. Aguiar-Hualde, and C. Bena, Majorana bound states in open quasi-one-dimensional and two-dimensional systems with transverse Rashba coupling, *Phys. Rev. B* **93**, 155425 (2016).
- [39] C. Bena, Testing the formation of Majorana states using Majorana polarization, *Comptes Rendus. Physique* **18**, 349 (2017).
- [40] V. Kaladzhyan, J. Despres, I. Mandal, and C. Bena, Majorana fermions in finite-size strips with in-plane magnetic fields, *Eur. Phys. J. B* **90**, 10.1140/epjb/e2017-80103-y (2017).
- [41] A. Y. Kitaev, Unpaired Majorana fermions in quantum wires, *Phys.-Usp.* **44**, 131 (2001).
- [42] S. Nadj-Perge, I. K. Drozdov, B. A. Bernevig, and A. Yazdani, Proposal for realizing Majorana fermions in chains of magnetic atoms on a superconductor, *Phys. Rev. B* **88**, 020407 (2013).
- [43] S. Cheng, Y. Zhu, G. Xianlong, and T. Liu, Fate of majorana zero modes by a modified real-space-pfaffian method and mobility edges in a one-dimensional quasiperiodic lattice, arXiv:2102.00737 .
- [44] T. Liu, S. Cheng, H. Guo, and G. Xianlong, Fate of Majorana zero modes, exact location of critical states, and unconventional real-complex transition in non-Hermitian

- quasiperiodic lattices, *Phys. Rev. B* **103**, 104203 (2021).
- [45] O. A. Awoga, I. Ioannidis, A. Mishra, M. Leijnse, M. Trif, and T. Posske, Controlling majorana hybridization in magnetic chain-superconductor systems, *Phys. Rev. Res.* **6**, 033154 (2024).
- [46] It is worth mentioning that the Majorana polarization has been also explored in the many-body context [55, 60–64], with a definition that differs but aims to characterize the same properties of MZMs. Similarly, the Majorana polarization has been used to characterize higher order topological superconductors [65]. We note that our definition in Eqs. (4) and (5) has now been adopted to distinguishing between MBSs and other zero-energy modes in quasicrystals [66].
- [47] R. M. Lutchyn, E. P. A. M. Bakkers, L. P. Kouwenhoven, P. Krogstrup, C. M. Marcus, and Y. Oreg, Majorana zero modes in superconductor-semiconductor heterostructures, *Nat. Rev. Mater.* **3**, 52 (2018).
- [48] H. Zhang, M. W. A. de Moor, J. D. S. Bommer, D. Xu, G. Wang, N. van Loo, C.-X. Liu, S. Gazibegovic, J. A. Logan, D. Car, R. L. M. O. h. Veld, P. J. van Veldhoven, S. Koelling, M. A. Verheijen, M. Pendharkar, D. J. Pennachio, B. Shojaei, J. S. Lee, C. J. Palmstrøm, E. P. A. M. Bakkers, S. D. Sarma, and L. P. Kouwenhoven, Large zero-bias peaks in InSb-Al hybrid semiconductor-superconductor nanowire devices (2021).
- [49] S. Ahn, H. Pan, B. Woods, T. D. Stanescu, and S. Das Sarma, Estimating disorder and its adverse effects in semiconductor Majorana nanowires, *Phys. Rev. Materials* **5**, 124602 (2021).
- [50] F. Nichele, A. C. C. Drachmann, A. M. Whiticar, E. C. T. O’Farrell, H. J. Suominen, A. Fornieri, T. Wang, G. C. Gardner, C. Thomas, A. T. Hatke, P. Krogstrup, M. J. Manfra, K. Flensberg, and C. M. Marcus, Scaling of Majorana zero-bias conductance peaks, *Phys. Rev. Lett.* **119**, 136803 (2017).
- [51] S. Das Sarma, In search of Majorana, *Nat. Phys.* **19**, 165–170 (2023).
- [52] P. San-Jose, E. Prada, and R. Aguado, ac josephson effect in finite-length nanowire junctions with Majorana modes, *Phys. Rev. Lett.* **108**, 257001 (2012).
- [53] J. Cayao, P. San-Jose, A. M. Black-Schaffer, R. Aguado, and E. Prada, Majorana splitting from critical currents in josephson junctions, *Phys. Rev. B* **96**, 205425 (2017).
- [54] J. Cayao, A. M. Black-Schaffer, E. Prada, and R. Aguado, Andreev spectrum and supercurrents in nanowire-based SNS junctions containing Majorana bound states, *Beilstein J. Nanotechnol.* **9**, 1339 (2018).
- [55] A. Tsintzis, R. S. Souto, K. Flensberg, J. Danon, and M. Leijnse, Majorana qubits and non-abelian physics in quantum dot-based minimal Kitaev chains, *PRX Quantum* **5**, 010323 (2024).
- [56] G. E. Blonder, M. Tinkham, and T. M. Klapwijk, Transition from metallic to tunneling regimes in superconducting microconstrictions: Excess current, charge imbalance, and supercurrent conversion, *Phys. Rev. B* **25**, 4515 (1982).
- [57] R. Pawlak, M. Kisiel, J. Klinovaja, T. Meier, S. Kawai, T. Glatzel, D. Loss, and E. Meyer, Probing atomic structure and majorana wavefunctions in mono-atomic fe chains on superconducting pb surface, *npj Quantum Information* **2**, 10.1038/npjqi.2016.35 (2016).
- [58] M. Leijnse and K. Flensberg, Parity qubits and poor man’s Majorana bound states in double quantum dots, *Phys. Rev. B* **86**, 134528 (2012).
- [59] T. Dvir, G. Wang, N. van Loo, C.-X. Liu, G. P. Mazur, A. Bordin, S. L. Ten Haaf, J.-Y. Wang, D. van Driel, F. Zatelli, X. Li, F. K. Malinowski, S. Gazibegovic, G. Badawy, E. P. A. M. Bakkers, M. Wimmer, and L. P. Kouwenhoven, Realization of a minimal Kitaev chain in coupled quantum dots, *Nature* **614**, 445 (2023).
- [60] S. V. Aksenov, A. O. Zlotnikov, and M. S. Shustin, Strong Coulomb interactions in the problem of Majorana modes in a wire of the nontrivial topological class BDI, *Phys. Rev. B* **101**, 125431 (2020).
- [61] A. Tsintzis, R. S. Souto, and M. Leijnse, Creating and detecting poor man’s Majorana bound states in interacting quantum dots, *Phys. Rev. B* **106**, L201404 (2022).
- [62] C.-X. Liu, A. M. Bozkurt, F. Zatelli, S. L. D. ten Haaf, T. Dvir, and M. Wimmer, Enhancing the excitation gap of a quantum-dot-based Kitaev chain, *arXiv:2310.09106* .
- [63] R. S. Souto, A. Tsintzis, M. Leijnse, and J. Danon, Probing Majorana localization in minimal Kitaev chains through a quantum dot, *Phys. Rev. Res.* **5**, 043182 (2023).
- [64] W. Samuelson, V. Svensson, and M. Leijnse, Minimal quantum dot based Kitaev chain with only local superconducting proximity effect, *Phys. Rev. B* **109**, 035415 (2024).
- [65] R. Arouca, T. Nag, and A. M. Black-Schaffer, Mixed higher-order topology, and nodal and nodeless flat band topological phases in a superconducting multiorbital model, *Phys. Rev. B* **110**, 064520 (2024).
- [66] A. Kobińska, O. A. Awoga, M. Leijnse, T. Domański, P. Holmval, and A. M. Black-Schaffer, Topological superconductivity in Fibonacci quasicrystal, *arXiv:2405.12178* .